DOI 10.5012/bkcs.2009.30.12.3021

Energy Band Structure and Photocatalytic Property of Fe-doped Zn_2TiO_4 Material

Jum Suk Jang,[†] Pramod H. Borse,[†,‡] Jae Sung Lee,[†] Kwon Taek Lim,[§] Ok-Sang Jung,[#] Euh Duck Jeong,[⊥] Jong Seong Bae,[⊥] Mi Sook Won,[⊥] and Hyun Gyu Kim[⊥,*]

[†]*Department of Chemical Engineering, Pohang University of Science and Technology, Pohang 790-784, Korea*
[‡]*Centre for Nanomaterials, International Advanced Research Centre for Powder Metallurgy and New Materials (ARC International), Balapur PO, Hyderabad, AP, 500 005, India*
[§]*Department of Imaging System Engineering, Pukyong National University, Busan 609-735, Korea*
[#]*Department of Chemistry (BK21), Pusan National University, Busan 627-706, Korea*
[⊥]*Busan Center, Korea Basic Science Institute, Busan 609-735, Korea. *E-mail: hhgkim@kbsi.re.kr*
Received September 1, 2009, Accepted November 4, 2009

$Zn_2Ti_{1-x}Fe_xO_4$ ($0 \le x \le 0.7$) photocatalysts were synthesized by polymerized complex (PC) method and investigated for its physico-chemical as well as optical properties. $Zn_2Ti_{1-x}Fe_xO_4$ can absorb not only UV light but also visible light region due to doping of Fe in the Ti site of Zn_2TiO_4 lattice because of the band transition from Fe 3d to the Fe 3d + Ti3d hybrid orbital. The photocatalytic activity of Fe doped Zn_2TiO_4 samples for hydrogen production under UV light irradiation decreased with an increase in Fe concentration in Zn_2TiO_4. Consequently, there exists an optimized concentration of iron for improved photocatalytic activity under visible light ($\lambda \ge 420$ nm)

Key Words: Fe doped Zn_2TiO_4, Polymerized complex method, Photocatalysis, Visible light, Hydrogen production

Introduction

Photocatalysts could convert solar energy into chemical energy by producing hydrogen gas from water or hydrogen containing compounds.[1-5] Thus hydrogen production by use of photocatalysts has recently received much attention because of the depletion of fossil fuel source and related environmental problems. Zn_2TiO_4 has been a promising material for the photocatalytic water splitting as well as photocatalytic oxidation reaction under UV light because of its higher reduction potential and lower oxidation potential.[6]

But, Zn_2TiO_4 has a wide band gap (3.1 eV) and thus don't show the photocatalytic activity under visible light.[6] Since visible light accounts for the largest portion (*ca.* 46%) of the solar spectrum, visible light-driven photocatalysts are needed for hydrogen production from water as well as the decomposition of toxic compounds. One promising approach to develop new photocatalysts is the tuning or modification of the optical properties of UV light active catalysts by doping, as demonstrated in $La_2Ti_{2-x}MxO_7$ (M = Fe, Cr),[7] Zr-S co-doped TiO_2,[8] $SrTi_xM_{1-x}O_3$ (M = Ru, Rh, Ir, Pt, Pd),[9] $TiO_{2-x}Cr_xO_2$,[10] $AgGa_{1-x}In_xS_2$,[11] $TiO_{2-x}C_x$,[12,13] or $TiO_{2-x}N_x$[14] for cation and anion doping.

Here we have tailored the band gap of Zn_2TiO_4 by doping of Fe metal ion with Ti site in Zn_2TiO_4 crystal lattice using the polymerized complex reaction and characterized it using UV-Vis diffuse reflectance spectroscopy (UV-Vis DRS) and X-ray diffraction (XRD). This work further reports the photocatalytic activity for hydrogen production under UV and visible light irradiation ($\lambda > 420$ nm).

Experimental

Preparation of nanocrystalline $Zn_2Ti_{1-x}Fe_xO_4$ ($0 \le x \le 0.7$). Nanocrystalline $Zn_2Ti_{1-x}Fe_xO_4$ was synthesiszed by the PC method according to the same procedure in our previous work.[15,16] Zinc nitrate hexahydrate ($Zn(NO_3)_2{\cdot}6H_2O$, 98.0%, Aldrich), iron nitrate hydrate ($Fe(NO_3)_3{\cdot}9H_2O$, 98%, Aldrich), titanium (IV) isopropoxide ($Ti[OCH(CH_3)_2]_4$, 97%, Aldrich), ethylene glycol ($C_2H_6O_2$, Kanto Chemicals), citric acid ($C_6H_8O_7$, Wako) were used as starting materials. The citric acid (CA) was added into ethylene glycol under constant agitation, at temperature of 60 - 70 °C. Ethylene glycol (EG) was added to the mixture to yield a mass proportion of 60% CA to 40% EG. Next, titanium (IV) isopropoxide was dissolved in citric acid-EG solution and then the salts of zinc nitrate hexahydrate and iron nitrate hydrate were dissolved in the above mixture to obtain metal citrate complex. Finally, the mixture was kept on the hot plate (80 °C) until it became a transparent solution. The well mixed solution was then heated at 130 °C for several hours to obtain a polymeric gel. The viscous polymeric product was pyrolyzed at about 300 - 500 °C to form the precursor powders. Thus obtained powder was pressed in the form of pellets, which were calcined at 1200 °C for 5 h in an electric furnace to obtain nanocrystalline $Zn_2Ti_{1-x}Fe_xO_4$. On the other hand, for the purpose of comparison, $TiO_{2-x}N_x$ nanoparticle was also prepared by the hydrolytic synthesis method (HSM).[17]

Characterization. $Zn_2Ti_{1-x}Fe_xO_4$ ($0 \le x \le 0.7$) samples thus obtained were characterized by X-ray Diffractometer (Mac Science Co., M18XHF). X-ray diffraction (XRD) results were compared with the Joint Committee Powder Diffraction Standards (JCPDS) data for phase identification. The band gap energy and optical property of the as-prepared materials was measured by UV-Visible diffuse reflectance spectrometer (Shimadzu, UV 2401). The morphology was determined by scanning electron microscopy (SEM, Hitachi, S-2460N) and high-resolution transmission electron microscopy (HR-TEM, Philips, CM 200).

Photocatalytic activity. The rate of H_2 evolution was determined for water-methanol solution (distilled water 70 mL and

methanol 30 mL) containing 0.1 g catalyst. The concentration of H_2 was analyzed by gas chromatography equipped with a thermal conductivity detector (molecular sieve 5-A column and Ar carrier). Before both reactions, 1 wt% of Pt was deposited on photocatalysts by photodeposition method under uv ($\lambda \geq$ 210 nm) and visible light ($\lambda \geq 400$ nm).

Results and Discussion

Structural characterization of the samples was investigated to compare their crystallization behaviors with respect to the calcination temperatures. Figure 1 shows the XRD patterns of $Zn_2Ti_{1-x}Fe_xO_4$ ($0 \leq x \leq 0.7$) samples prepared by the conventional solid state reaction method. All the samples showed an inverse spinel with a lattice constant of 8.48 Å and space group Fd3m.[18] But, undoped Zn_2TiO_4 and $Zn_2Ti_{0.95}Fe_{0.05}O_4$ samples represent pure crystal structure without Fe_2O_3 crystal phase among the as-synthesized samples. With the increase in the concentration of iron ($x = 0.05$), X-ray diffraction pattern of Fe_2O_3 in $Zn_2Ti_{1-x}Fe_xO_4$ ($0.1 \leq x \leq 0.7$) samples clearly appear the Figure 1. This indicates that only small amount of iron ion into Zn_2TiO_4 crystal structure can be substituted into the lattice of Ti site in Zn_2TiO_4 crystal structure.

The optical properties were studied by UV-Vis diffuse reflectance (UV-DR) spectroscopy for iron doped Zn_2TiO_4 samples with different contents. Figure 2 shows the UV-Visible diffuse reflectance spectra of $Zn_2Ti_{1-x}Fe_xO_4$ ($0 \leq x \leq 0.7$) samples ($0 \leq x \leq 0.7$). In case of undoped Zn_2TiO_4 sample, absorption edge appeared near 400 nm corresponding to 3.1 eV, consistent with the literature.[6] However, the absorption spectra of Fe doped Zn_2TiO_4 samples exhibit new absorption shoulder in visible light region. In general, the absorption edge of Zn_2TiO_4 around 400 nm was ascribed to the band transition from O 2p to Zn 4s. Additionally, the absorption of Fe doped Zn_2TiO_4 samples was based on the transition from Fe e_g to Fe 4s. In this case, the interband may exist between the conduction and valence band of Zn_2TiO_4.

Figure 3 shows scanning electron microscopy (SEM) images of $Zn_2Ti_{1-x}Fe_xO_4$ ($x = 0.0, 0.05, 0.1, 0.2$) samples with different content of iron calcined at 1200 °C for 5 h, respectively. All samples represent the morphology of a well-developed crystal and the grain size of as-synthesized samples shows a similar value of 5 ~ 10 μm. But, with increasing the Fe doping level into the lattice site of Ti in Zn_2TiO_4 crystal structure, there exists the impurity crystal phase with small grain size. The existence of small grains possibly affects the photocatalytic activity of as-prepared samples.

We investigated the photocatalytic hydrogen production from methanol-water solution using undoped Zn_2TiO_4 and $Zn_2Ti_{1-x}Fe_xO_4$ ($x = 0.05, 0.1$), and $TiO_{2-x}N_x$ samples under uv and visible light irradiation. Table 1 shows the results of H_2 evolution as well as respective band gaps of the samples calculated from respective DRS spectra. All the samples showed the photocatalytic activity for hydrogen production from methanol-water solution under uv light irradiation ($\lambda \geq 210$). Among the as-synthesized samples, undoped Zn_2TiO_4 photocatalyst showed the highest photocatalytic activity as compared to other samples. The Fe doped sample, $Zn_2Ti_{0.95}Fe_{0.05}O_4$, with low doping level only showed H_2 production as high as 6.2 mmol/gcat·hr under visible

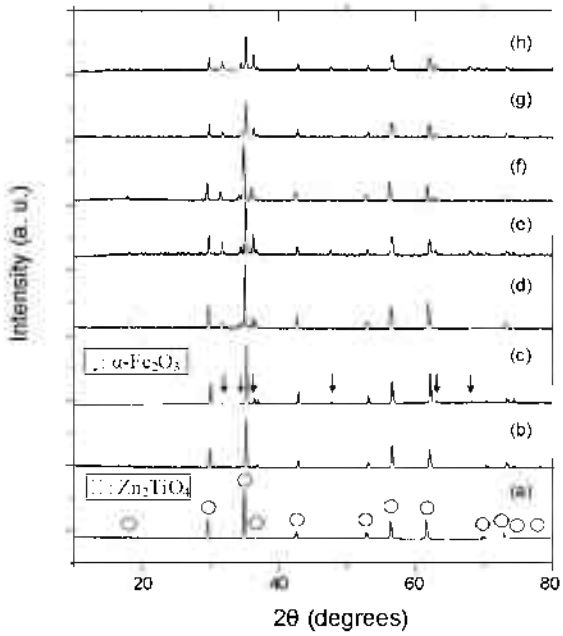

Figure 1. X-ray diffraction patterns of $Zn_2Ti_{1-x}Fe_xO_4$ photocatalysts for x = (a) 0, (b) 0.05, (c) 0.1, (d) 0.2, (e) 0.3, (f) 0.4, (g) 0.6, and (h) 0.7.

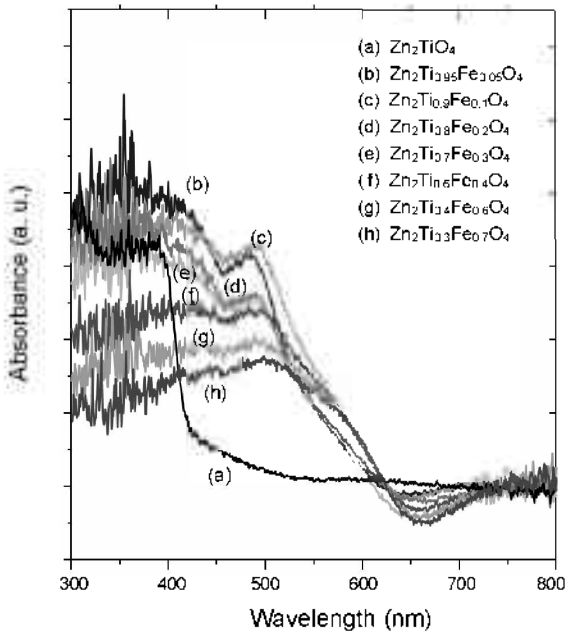

Figure 2. UV-vis diffuse reflectance spectra of $Zn_2Ti_{1-x}Fe_xO_4$ photocatalysts for x = (a) 0, (b) 0.05, (c) 0.1, (d) 0.2, (e) 0.3, (f) 0.4, (g) 0.6, and (h) 0.7.

light irradiation ($\lambda \geq 420$ nm). But, $Zn_2Ti_{0.9}Fe_{0.1}O_4$ and $TiO_{2-x}N_x$ samples showed a trace amount of H_2 production. This indicates that the $Zn_2Ti_{0.95}Fe_{0.05}O_4$ seems to be an optimum concentration which could lead to the proper bandgap as well as band position for producing hydrogen gas as compared to other samples. Possibly, the Fe doping concentration higher than $Zn_2Ti_{0.95}Fe_{0.05}O_4$ ($x = 0.05$) leads to Fe_2O_3 as an impurity phase, which could play a role of electron transfer medium towards a positive

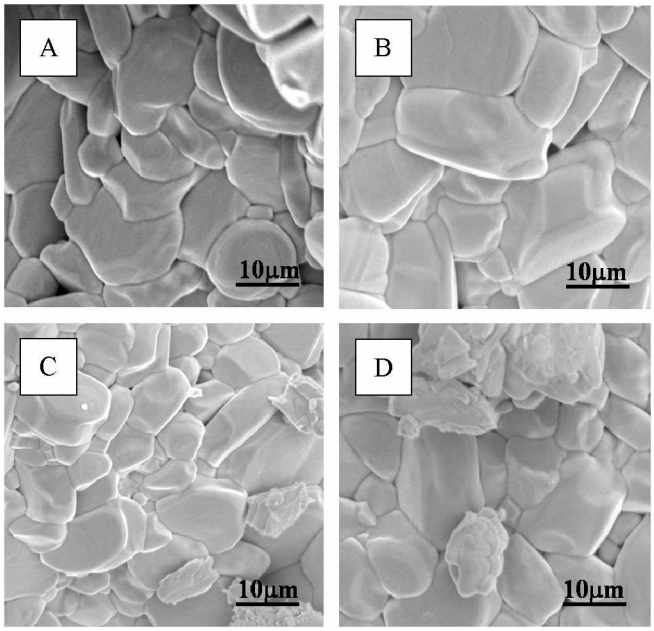

Figure 3. SEM images of $Zn_2Ti_{1-x}Fe_xO_4$ samples for x = (a) 0, (b) 0.05, (c) 0.1, and (d) 0.2.

Table 1. Photocatalytic H_2 production from methanol-water solution over 1wt% $Pt/ZnTi_{1-x}Fe_xO_4$ (x = 0.0, 0.05, 0.1) and 1wt% $Pt/TiO_{2-x}N_x$ samples.

Catalyst	Energy band gap		H_2 evolution (mmol/gcat.hr)	
	Eg (eV)-1	Eg (eV)-2	UV light irradiation ($\lambda > 210$ nm)	Visible lihgt irradiation ($\lambda > 420$ nm)
Pt/Zn_2TiO_4	3.10	-	140	0
$Pt/Zn_2Ti_{0.95}Fe_{0.05}O_4$	3.10	2.48	116	6.2
$Pt/Zn_2Ti_{0.9}Fe_{0.1}O_4$	3.10	2.48	11	Trace
$Pt/TiO_{2-x}N_x$	3.20	2.73	8	Trace

potential more than the reduction potential of H_2.

Figure 4 shows time curve of the photocatalytic hydrogen production over $Zn_2Ti_{0.95}Fe_{0.05}O_4$ for 15 h with intermittent N_2 gas purging every 3 h (dotted line). There was no noticeable reduction in activity during the first two runs for 6 h. This implies that the $Zn_2Ti_{0.95}Fe_{0.05}O_4$ sample may be stable in water-methanol solution during photocatalytic reaction.

XPS measurements were carried out to analyze the oxidation state of Fe atoms in $Zn_2Ti_{0.95}Fe_{0.05}O_4$ photocatalyst. Figure 5 shows the XPS survey spectrum of $Zn_2Ti_{0.95}Fe_{0.05}O_4$ sample, which contains Zn, Ti, O, C and Fe elements, with photoelectron peaks appearing at binding energies of 1022 (Zn $2p_{3/2}$), 459 (Ti $2p_{3/2}$), 531 (O 1s) and 285 eV (C 1s) and a weak photoelectron peak at 711 eV (Fe $2p_{3/2}$). The inset in Figure 5 presents the core level spectra of the Fe $2p_{3/2}$ region of corresponding sample revealing that the peak at 711 eV is symmetrical and can be ascribed to the trivalent oxidation state of Fe (Fe^{3+}).

Figure 6A shows the bandgap position of $Zn_2Ti_{0.95}Fe_{0.05}O_4$ and $TiO_{2-x}N_x$ photocatalysts as suggested from the results of

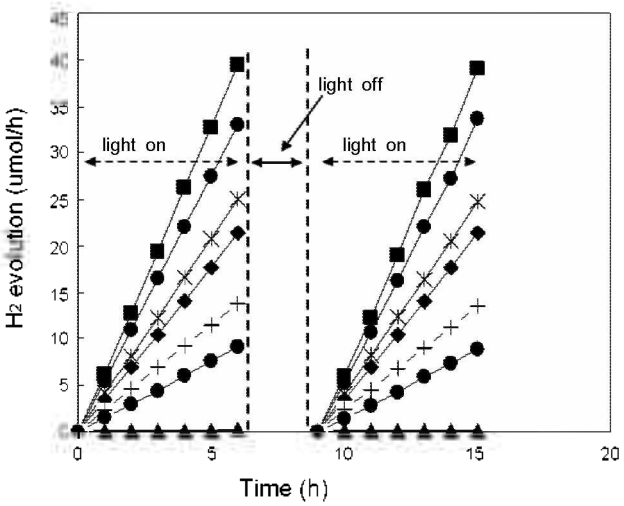

Figure 4. Time courses of hydrogen production over various $Zn_2Ti_{1-x}Fe_xO_4$ for x = (■) 0.05, (●) 0.04, (×) 0.06, (◆) 0.07, (+) 0.03, (○) 0.02 and (▲), $TiO_{2-x}N_x$ photocatalysts.

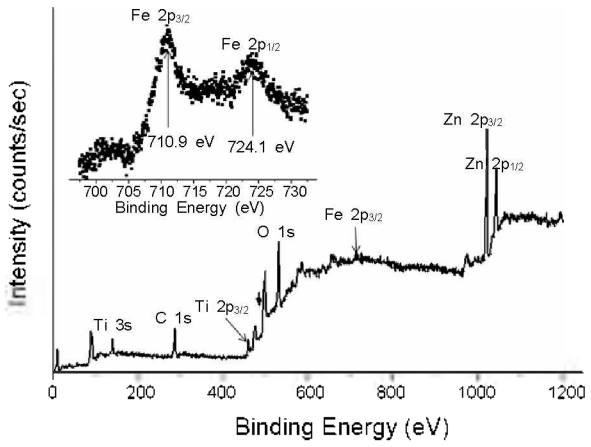

Figure 5. XPS survey spectrum of $Zn_2Ti_{0.95}Fe_{0.05}O_4$ sample. The insert shows the XPS core-level spectra of Fe 3d in $Zn_2Ti_{0.95}Fe_{0.05}O_4$ sample.

undoped Zn_2TiO_4 and TiO_2 reported by Matsumoto *et al.*[6] and UV-DRS data of doped two materials.[15] The bandgap energy of $Zn_2Ti_{0.95}Fe_{0.05}O_4$ and $TiO_{2-x}N_x$ are *ca.* 2.48, 2.73 eV, respectively. In general, in case of Fe-doped material an interband is formed between the conduction and valence band of undoped material.[7] Thus, the doped material could absorb visible light due to the transition from interband to the conduction band of the original material. With knowledge of the band position of the undoped material, here we propose the schematic of band positions of doped material as shown in Figure 6A. Figure 6B represents the schematic describing the mechanism for photocatalytic hydrogen production over $Zn_2Ti_{0.95}Fe_{0.05}O_4$ from methanol-water solution under visible light irradiation ($\lambda \geq 420$ nm). $Zn_2Ti_{0.95}Fe_{0.05}O_4$ photocatalyst produced H_2 gas in the presence of aqueous methanol-water solution under visible light. Thus, in the case of Pt/Fe-doped Zn_2TiO_4, an electron excited is to the conduction band due to sufficiently high reduction potential to reduce H^+ ion and a hole in the valence band also has lower oxidation potential for CH_3OH degradation to CO_2. H_2 gas was

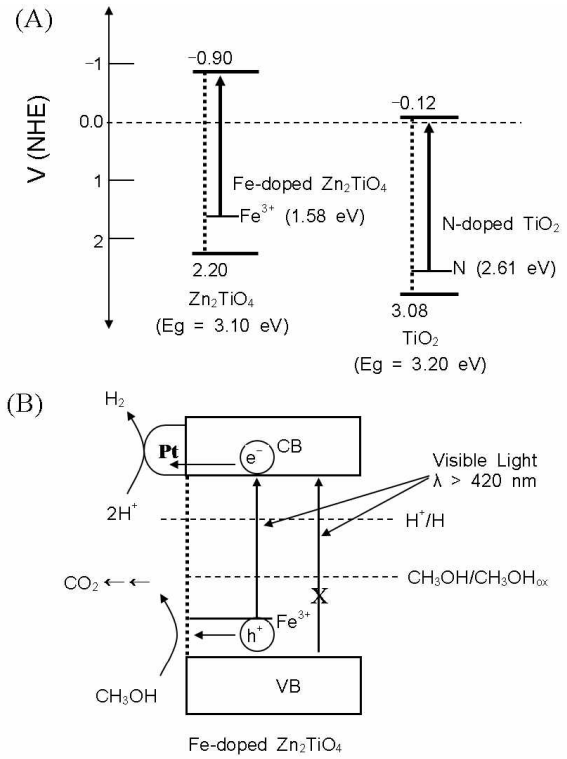

Figure 6. (A) The bandgap position of $Zn_2Ti_{1-x}Fe_xO_4$ and $TiO_{2-x}N_x$ photocatalysts. (B) The schematic describing the mechanism for photocatalytic hydrogen production from methanol-water solution.

generated only when the formation of an ohmic junction between Pt and Fe doped Zn_2TiO_7 might enhance the charge separation. Therefore, Fe doped Zn_2TiO_4 could be applied for photocatalytic reaction that requires a higher reduction potential as well as lower oxidation potential.

Conclusions

$Zn_2Ti_{1-x}Fe_xO_4$ photocatalysts were successfully prepared by the polymerized complex method. New band gap in the visible light range was obtained by Fe doping in Zn_2TiO_4. $Zn_2Ti_{0.95}Fe_{0.05}O_4$ sample with low doping level was synthesized without impurity phase such as Fe_2O_3 and only showed the photocatalytic activity under visible light irradiation ($\lambda \geq 420$ nm). Further increase of the amount of Fe in Zn_2TiO_4 led to the formation of Fe_2O_3 crystal phase. Therefore, it is considered that Fe doping could play an important role in reducing the bandgap and showing the photocatalytic activity in the system of Zn_2TiO_4 under visible light irradiation.

Acknowledgments. This work has been supported by KBSI grant T29320, MKE-RTI04-0201, KOSEF grant (NCRCP, R15-2006-022-01002-0), Hydrogen Energy R&D Center, Korea.

Reference

1. Lee, J. S. *Catal. Surv. Asia.* **2005**, *9*, 217.
2. Kudo, A.; Miseki, Y. *Chem. Soc. Rev.* **2009**, *38*, 253.
3. Maeda, K.; Takata, T.; Hara, M.; Saito, N.; Inoue, Y.; Kobayashi, H.; Domen, K. *J. Am. Chem. Soc.* **2005**, *127*, 8286.
4. Kim, H. G.; Hwang, D. W.; Lee, J. S.; J. *Am. Chem. Soc.* **2004**, *126*, 8913.
5. Jang, J. S.; Ji, S. M.; Bae, S. W.; Son, H. C.; Lee, J. S. J. *Photochem. Photobiol. A: Chem.* **2007**, *188*, 112.
6. Matsumoto, Y. *J. Solid State Chem.* **1996**, *126*, 227.
7. Hwang, D. W.; Kim, H. G.; Lee, J. S.; Kim, J.; Li, W.; Oh, S. H.; *J. Phys. Chem.* **2005**, *B109*, 2093.
8. Kim, S. W.; Khan, R.; Kim, T. J.; Kim, W. *Bull. Korean Chem. Soc.* **2008**, *29*, 1217.
9. Bae, S. W.; Borse, P. H.; Lee, J. S. *Appl. Phys. Lett.* **2008**, *92*, 104107.
10. Bae, S. W.; Borse, P. H.; Hong, S. J.; Jang, J. S.; Lee, J. S.; Jeong, E. D.; Hong, T. E.; Yoon, J. H.; Jin, J. S.; Kim, H. G. *J. Korean Phys. Soc.* **2007**, *51*, S22.
11. Subramanian, E.; Baeg, J.; Kale, B. B.; Lee, S. M.; Moon, S.; Kong, K. *Bull. Korean Chem. Soc.* **2007**, *28*, 2089.
12. Khan, S. U.; Al-Shahry, M. M.; Ingler, Jr., W. B. *Science* **2002**, *297*, 2243.
13. Sakthivel, S.; Kisch, H.; *Angew. Chem. Int. Ed.* **2003**, *42*, 4908.
14. Ashai, R.; Ohwaki, T.; Aoki, K.; Taga, Y. *Science* **2001**, *293*, 269.
15. Kim, H. G.; Hwang, D. W.; Bae, S. W.; Jung, J. H.; Lee, J. S. *Catal. Lett.* **2003**, *91*, 193.
16. Jung, E. D.; Borse, P. H.; Jang, J. S.; Lee, J. S.; Cho, C. R.; Bae, J. S.; Park, S.; Jung, O. S.; Ryu, S. M.; Kim, H. G. *J. Nanosci. Nanotech.* **2008**, *9*, 3568 .
17. Jang, J. S.; Kim, H. G.; Ji, S. M.; Bae, S. W.; Jung, J. H.; Shon, B. H.; Lee, J. S. *J. Solid State Chem.* **2006**, *179*, 1067.
18. Rankin, R. B.; Campos, A.; Tian, H.; Siriwardane, R.; Roy, A.; Spivey, J. J.; Sholl, D. S.; Johnson, J. K. *J. Am. Ceram. Soc.* **2008**, *91*, 584.